

**Optimization of Pressure Swing Adsorption and Fractionated Vacuum  
Pressure Swing Adsorption Processes for CO<sub>2</sub> Sequestration**

*Daeho Ko<sup>1)</sup>, Ranjani Siriwardane<sup>2)</sup> and Lorenz T. Biegler<sup>1)</sup>*

*<sup>1)</sup> Department of Chemical Engineering  
Carnegie Mellon University  
Pittsburgh, PA 15213*

*<sup>2)</sup> National Energy Technology Laboratory  
U.S. Department of Energy  
Morgantown, WV 26507*

Key words: optimization, PSA, FVPSA, CO<sub>2</sub> sequestration, cyclic steady state

Prepared for Presentation at the 2004 AIChE Annual Meeting, Austin Convention  
Center  
Austin, TX, November 7-12  
PSA/TSA

Copyright © Daeho Ko, Ranjani V. Siriwardane, and Lorenz T. Biegler  
November 2004

Unpublished

AIChE shall not be responsible for statements or opinions contained in papers or  
printed in its publications

## Abstract

This work focuses on the optimization of cyclic adsorption processes to improve the performance of CO<sub>2</sub> sequestration from flue gas consisting of nitrogen and carbon dioxide. The adopted processes are the PSA (pressure swing adsorption) process and the FVPSA (fractionated vacuum pressure swing adsorption) process, which is modified from the FVSA (fractionated vacuum swing adsorption) process developed by Air Products and Chemicals, Inc. The systems adopt zeolite13x as an adsorbent. The high temperature PSA is better for high purity of the sequestered product (CO<sub>2</sub>) and the high temperature FVPSA is much better than the normal temperature PSA processes. The main goal of this study is to improve purities of both components (nitrogen and carbon dioxide). The Langmuir isotherm parameters were calculated from the experimental data of NETL [1]. To perform optimization work more efficiently, we modified the previous optimization method by Ko et al. [2, 3] and obtained the optimization results with more accurate cyclic steady states (CSS) and better convergence as well as faster computation. As a result, the optimal conditions at CSS are found for these systems.

## 1. Introduction

As discussed in [4, 5], almost 42 % of industrial CO<sub>2</sub> emissions are from energy conversion. Because the CO<sub>2</sub> accumulation of green house gases may seriously affect the global climate, efficient sequestration of carbon dioxide is very important. One way to mitigate CO<sub>2</sub> accumulation in the air is to capture CO<sub>2</sub> from the emission sources and inject it into the ocean [6]. Gas absorption has been used to recover CO<sub>2</sub>; however, this process is energy-consuming for the regeneration of solvent and has corrosion problems [7]. Recently, gas-solid adsorption processes may be applicable for the removal of CO<sub>2</sub> from power plant flue gas. A few cyclic adsorption processes are used commercially for the regeneration of CO<sub>2</sub> [8]. In pressure swing adsorption (PSA) and vacuum pressure swing adsorption (VPSA), the adsorbent is regenerated by decreasing the total or partial pressure. Thermal (or temperature) swing adsorption (TSA) regenerates the sorbent by increasing temperature. PSA processes have been suggested as an energy saving process and as an alternative to traditional separations, distillation and absorption [3], for bulk gas separations such as CO<sub>2</sub> sequestration. To dispose of CO<sub>2</sub> to the ocean or depleted oil fields, CO<sub>2</sub> needs to be highly concentrated [7]. In this sense, PSA or VPSA processes may be useful for the CO<sub>2</sub> concentration. The PSA operation has initially adopted the steps of the classical Skarstrom cycle [9]: pressurization with feed, adsorption with high pressure, depressurization, and purge. In the 1960s, a pressure equalization step was suggested to save repressurization energy after the purge step [10, 11, 12]. Since the 1980s, VSA has also been attractive in enhancing regeneration efficiency [13, 14, 15]. Among the many applications of PSA processes, the production of top product- and bottom product-enriched gases from feed gas is very important, but almost all the PSA processes produce only top product- or bottom product-enriched gases. This characteristic is based on the following reasons [16]. First, the total concentration of the strong adsorbate in the bed is not high, as the strong species is in the void space of the adsorbent. The released vent gas has only a high concentration of weak adsorbate, which is discarded. Consequently, in these PSA processes, only one product-enriched stream is produced at the feeding step. Air Products resolved this problem by using vacuum swing adsorption (VSA) process. The key technology of the VSA in air separation is to introduce a nitrogen-rinse step after the air adsorption step [17]. Moreover, in the 1990s, a fractionated vacuum swing adsorption (FVSA) process was developed by Air Products, which simultaneously produces a 98+% nitrogen-enriched gas and an 80-90% oxygen-enriched gas from ambient air [16, 18]. The FVSA process studied is a dual-bed four-step process which simultaneously produces concentrated oxygen and nitrogen with ambient air as the feed [16, 18].

Our previous work [3] treated the optimization of PSA to remove CO<sub>2</sub> and obtained a high N<sub>2</sub> purity; however, the previous model needs to be updated because its CO<sub>2</sub> purity was not high. So the current work adopts a new isotherm data ranging from 303.15K to 390.15K and optimizes three types of adsorption processes: a normal temperature PSA, a high temperature PSA and a modified

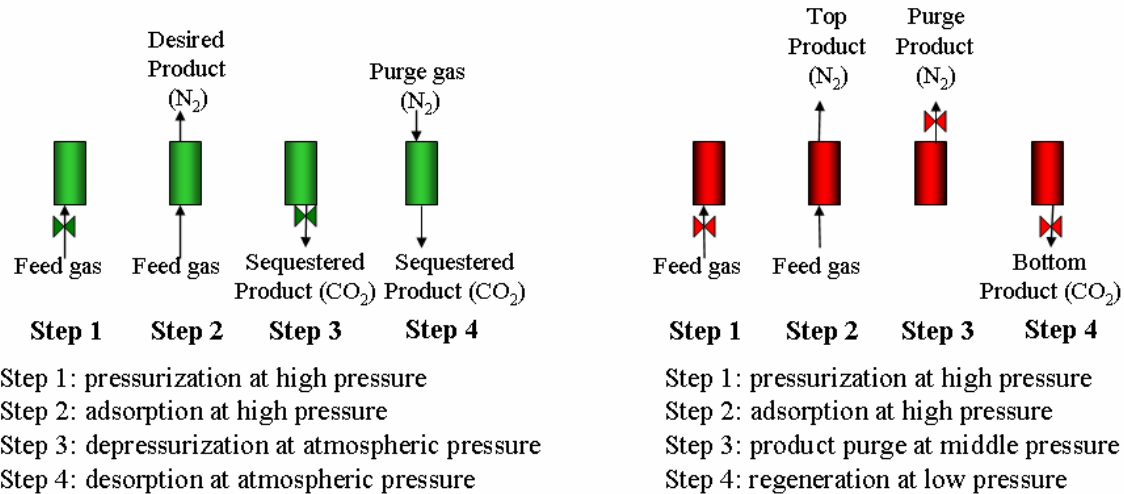
fractionated vacuum pressure swing adsorption (FVPSA) process, based on the FVSA concept, to improve the CO<sub>2</sub> purity as well as N<sub>2</sub> purity. The PSA operation adopts a Skarstrom cycle and the modified FVPSA operation consists of four steps: pressurization, adsorption, cocurrent blowdown and countercurrent regeneration. In FVPSA nitrogen is produced at the top of the bed during the adsorption and cocurrent blowdown steps, and carbon dioxide is obtained at the bottom of the bed during the countercurrent regeneration step. To calculate the gas velocity of the boundary during the pressure change step, valve equations are used [19]. This study presents an updated PSA optimization method from the previous one, called tailored single discretization (TSD) developed by Ko et al. (2002 and 2003) [2, 3], and performs the optimizations of the PSA and FVPSA processes.

## 2. Operations of target processes and the model equations

**2.1 Target processes.** The target processes are the PSA which is similar to the previous work [3] and FVPSA that is modified from the FVSA of Air Products. The adsorbent is zeolite13x and the feed gas consists of 85% nitrogen and 15% carbon dioxide. The parameters for the adsorption model are shown in Table 1. The operation cycles of the processes are shown in Figure 1.

The previous work [3] explains the PSA operation adopted in this study:

- (1) Pressurization step with feed gas at high pressure,
- (2) Adsorption step with feed gas producing N<sub>2</sub> at the top of the bed,
- (3) Depressurization step to atmospheric pressure (around 1atm) emitting the CO<sub>2</sub> at the bottom of the bed, and
- (4) Purge step with the carrier gas (pure N<sub>2</sub>) at atmospheric pressure (around 1atm) regenerating CO<sub>2</sub> from the adsorbent.



(a) PSA operation: Skarstrom cycle

(b) FVPSA operation

Figure 1. Four-step operation of PSA and FVPSA processes

The FVPSA operation also consists of four steps:

- (1) Pressurization step with feed at high pressure,
- (2) Adsorption step with feed at high pressure producing  $N_2$ ,
- (3) Cocurrent blowdown step (product purge step) at medium pressure (around 1atm) purging the top product ( $N_2$ ), and
- (4) Countercurrent blowdown step (countercurrent regeneration step) at low pressure (around 0.1~0.7atm) obtaining the sequestered product ( $CO_2$ ) at the bottom of the bed.

**Table1. Parameters for Adsorption Models**

Parameters	Values
Bed radius ( $R_{bed}$ )	$1.1 \times 10^{-2}$ m
Pore diameter ( $D_{pore}$ )	$1.0 \times 10^{-9}$ m
Particle radius ( $R_{particle}$ )	$1.0 \times 10^{-3}$ m
Bed density ( $\rho_{bed}$ )	$1.06 \times 10^3$ kg/m <sup>3</sup>
Wall density ( $\rho_{wall}$ )	$7.8 \times 10^3$ kg/m <sup>3</sup>
Bed void ( $\epsilon_{bed}$ )	0.348
Particle density ( $\rho_{particle}$ )	$1.87 \times 10^3$ kg/m <sup>3</sup>
R	8.314 J/mol/K
Heat capacity of solid ( $C_{ps}$ )	504 J/kg/K

**2.2 Model equations.** The following model assumptions and equations are adopted in this study. The current assumptions 1~5 are the same as the previous work [3] and assumptions 6-10 are different.

1. The gas phase follows ideal gas law.
2. Radial variation of temperature, pressure and concentration is neglected.
3. Competitive adsorption behaviors are described by the Langmuir equation for mixture gas.
4. The adsorption rate is approximated by the linear driving force (LDF) expression.
5. Physical properties of the bed are independent of the temperature.
6. Diffusion coefficient is affected by the temperature.
7. For all given superficial velocities, we assume that the axial pressure drop along the bed remains negligible.
8. In PSA operation, pressure within the bed is constant during the adsorption and desorption steps, and it is changed linearly according to time during the pressurization and depressurization step;

In FVPSA operation, pressure within the bed is constant during the adsorption step, and it is changed linearly according to the time during the pressurization, cocurrent blowdown, and regeneration steps.

9. The superficial velocity along the bed is calculated by nonisothermal overall mass balance equations during the constant pressure steps;
10. During the pressure change step the profile of the superficial velocity is linear along the bed and affected by the valve equation. From additional numerical experiments, we found this assumption to be reasonable.

The following dual-site Langmuir isotherm describes the adsorption equilibrium.

$$q_i^* = \frac{q_{mi(1)} b_{i(1)} P_i}{1 + \sum_{i=1}^n b_{i(1)} P_i} + \frac{q_{mi(2)} b_{i(2)} P_i}{1 + \sum_{i=1}^n b_{i(2)} P_i} \quad (1)$$

The isotherm parameters are calculated by the following equations (2a~2d) depending on the temperature, of which range is from 303.15K to 393.15K.

$$q_{mi(1)} = k_{1,i(1)} + k_{2,i(1)}T \quad (2a)$$

$$b_{i(1)} = k_{3,i(1)} \exp(k_{4,i(1)}/T) \quad (2b)$$

$$q_{mi(2)} = k_{1,i(2)} + k_{2,i(2)}T \quad (2c)$$

$$b_{i(2)} = k_{3,i(2)} \exp(k_{4,i(2)}/T) \quad (2d)$$

The isotherm parameter values, which are shown in Table 2, were obtained from experimental data taken at NETL. The isotherm parameter values calculated by using a nonlinear regression method agree well with the experimental data as shown in Figure 2. For the whole temperature range (303.15~393.15K), the selectivity of CO<sub>2</sub> over N<sub>2</sub> is very high as shown in Figure 2. Tables 3 and 4 list the model equations and mole flux variables to calculate the performances (purities and recoveries), respectively. The boundary conditions of each operating step are shown in Tables 5-1 and 5-2.

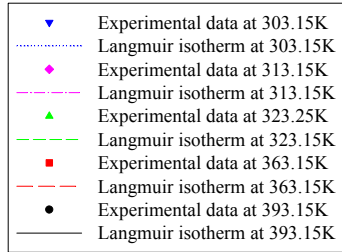
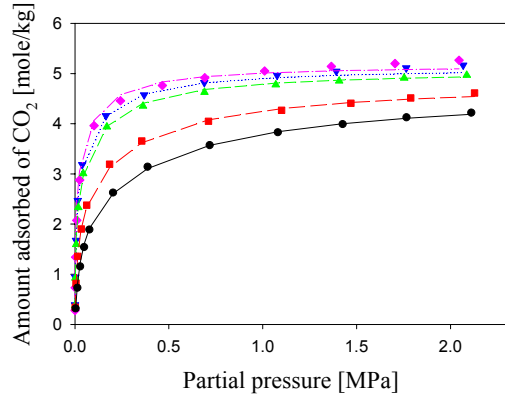
**Table 2. Values of parameters of the dual-site Langmuir isotherm**

	CO <sub>2</sub> (i=1)	N <sub>2</sub> (i=2)
$k_{1,i(1)}$	2.817269	1.889581045
$k_{2,i(1)}$	$-3.5 \times 10^{-4}$	$-22462 \times 10^{-4}$
$k_{3,i(1)}$	$2.83 \times 10^{-9}$	$1.163388 \times 10^{-9}$
$k_{4,i(1)}$	2,598.203	1,944.605788
$k_{1,i(2)}$	3.970888	1.889581045
$k_{2,i(2)}$	$-4.95 \times 10^{-3}$	$-2.2462 \times 10^{-4}$
$k_{3,i(2)}$	$4.411 \times 10^{-9}$	$1.163388 \times 10^{-9}$
$k_{4,i(2)}$	3,594.071	1,944.605788

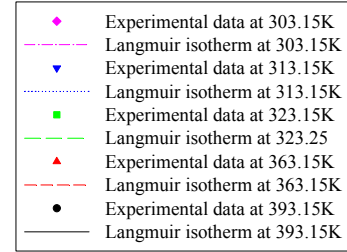
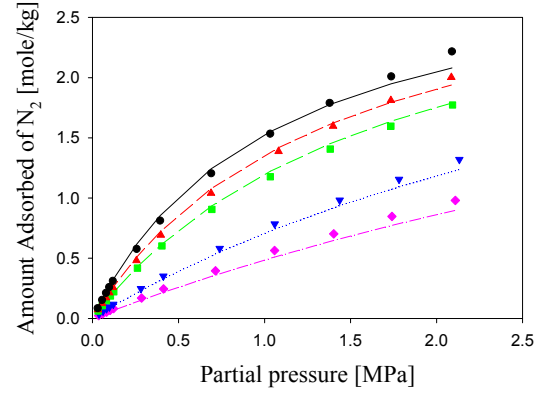
**Table 3. Model equations of PSA and FVPSA processes**

Component mass balance	$-D_x \left[ \frac{\partial^2 y_i}{\partial z^2} + 2T \left( \frac{\partial y_i}{\partial z} \right) \left\{ \frac{\partial}{\partial z} \left( \frac{1}{T} \right) \right\} \right] + \frac{\partial y_i}{\partial t} + u \frac{\partial y_i}{\partial z}$ $+ \frac{RT}{P} \frac{1 - \varepsilon_{bed}}{\varepsilon_{bed}} \rho_{particle} \left( \frac{\partial q_i}{\partial t} - y_i \sum_{i=1}^n \frac{\partial q_i}{\partial t} \right) = 0$ <span style="float: right;">(3)</span>
Overall mass balance	$\frac{\partial u}{\partial z} + \frac{1}{P} \frac{\partial P}{\partial t} + T \left\{ -D_x \frac{\partial}{\partial z^2} \left( \frac{1}{T} \right) + \frac{\partial}{\partial t} \left( \frac{1}{T} \right) + u \frac{\partial}{\partial z} \left( \frac{1}{T} \right) \right\}$ $+ \frac{\rho_{particle} RT}{P} \frac{1 - \varepsilon_{bed}}{\varepsilon_{bed}} \sum_{i=1}^n \frac{\partial q_i}{\partial t} = 0$ <span style="float: right;">(4)</span>
Linear driving force model	$\frac{\partial q_i}{\partial t} = \frac{15D_e}{R_{particle}} (q_i^* - q_i)$ <span style="float: right;">(5)</span>
Energy balance of the gas within the bed	$\left( \varepsilon_t \rho_{gas} C_{pg} + \rho_{bed} C_{ps} \right) \frac{\partial T}{\partial t} + \rho_{gas} C_{pg} \varepsilon_{bed} u \frac{\partial T}{\partial z} - K_L \frac{\partial^2 T}{\partial z^2}$ $- \rho_{bed} \sum_{i=1}^n \Delta H_i \frac{\partial q_i}{\partial t} + \frac{2h_i}{R_{bed}} (T - T_{wall}) = 0$ <span style="float: right;">(6)</span>
Isosteric heat of adsorption	$-\Delta H = R \left[ \frac{d \ln P}{d(1/T)} \right]_q$ <span style="float: right;">(7)</span>
Valve equation	$u = C_v \frac{R}{\varepsilon \pi R_b^2} \sqrt{\frac{T}{\sum_{i=1}^n y_i M w_i}} 1.1792486 \sqrt{\frac{P_{high}^2 - P_{low}^2}{P^2}}, \quad \text{if } P_{low} > 0.53 P_{high}$ $u = C_v \frac{R}{\varepsilon \pi R_b^2} \sqrt{\frac{T}{\sum_{i=1}^n y_i M w_i}} \frac{P_{high}}{P}, \quad \text{if } P_{low} \leq 0.53 P_{high}$ <span style="float: right;">(8)</span> <p>where,</p> <p><math>P_{high} \geq P_{low}</math></p> <p><math>P = P_{high}</math> if the gas stream is leaving the bed</p> <p><math>P = P_{low}</math> if the gas stream is entering the bed</p>

The valve equations of Table 3 are used to calculate the gas velocity during the pressure change steps, i.e., pressurization and depressurization steps for the PSA, and pressurization, cocurrent blowdown and countercurrent regeneration steps for FVPSA.



(a) Adsorption isotherm of CO<sub>2</sub>



(b) Adsorption isotherm of N<sub>2</sub>

Figure 2. Adsorption isotherms at different temperatures (303.15K~393.15K) on zeolite13x

Based on the mole flux variables of Table 4, the purities and recoveries of CO<sub>2</sub> (i=1) and N<sub>2</sub> (i=2) are calculated by

$$Purity_{CO_2,ave} = \frac{\int (Exhaust_{CO_2}) dt \Big|_{Exhaust\ step}}{\int \left( \sum_{i=1}^n Exhaust_i \right) dt \Big|_{Exhaust\ step}} \quad (9)$$

$$Purity_{N_2,ave} = \frac{\int (Product_{N_2}) dt \Big|_{Product\ step}}{\int \left( \sum_{i=1}^n Product_i \right) dt \Big|_{Product\ step}} \quad (10)$$

$$Recovery_{CO_2,ave} = \frac{\int Exhaust_{CO_2} dt \Big|_{exhaust\ step}}{\int Feed_{CO_2} dt \Big|_{feed\ step}} \quad (11)$$

$$Recovery_{N_2,ave} = \frac{\int Product_{N_2} \Big|_{Product\ step}}{\int Feed_{N_2} \Big|_{feed\ step}} \quad (12)$$

where:

Feed step of PSA and FVPSA = pressurization and adsorption step;

Product step of PSA = adsorption step for PSA;

Product step of FVPSA = adsorption and cocurrent blowdown step;

Exhaust step of PSA = depressurization and regeneration steps;

Exhaust step of FVPSA = regeneration step.

The work to compress the feed gas is given by

$$Power = \frac{\gamma}{\gamma-1} RT_{feed} \left( \left( \frac{P_{feed}}{P_{atm}} \right)^{\frac{\gamma-1}{\gamma}} - 1 \right) u(0) \pi (R_{bed})^2 \frac{P_{feed}}{RT_{feed}} \quad (13)$$

$$W_{cycle} = \int_0^{t_p+t_A} (Power) dt \quad (14)$$

$$Power_{ave} = \frac{W_{cycle}}{t_p + t_A} \quad (15)$$

$$Specific\ Power = \frac{\gamma}{\gamma-1} RT_{feed} \left( \left( \frac{P_{feed}}{P_{atm}} \right)^{\frac{\gamma-1}{\gamma}} - 1 \right) \quad (16)$$

$$Specific\ Work = \int_0^{t_p+t_A} (Specific\ Power) dt \quad (17)$$

$$Specific\ Power_{ave} = \frac{Specific\ Work}{t_p + t_A} \quad (18)$$

**Table 4-1. Mole flux variables at each operating step of PSA [3]**

Pressurization	Adsorption	Depressurization	Purge
$\frac{\partial(Feed_i)}{\partial t}$ $= \frac{uP_i}{RT} \Big _{z=0} \left[ \frac{T _{z=0}}{T_{STP}} \frac{P_{STP}}{P} \right]$	$\frac{\partial(Feed_i)}{\partial t}$ $= \frac{uP_i}{RT} \Big _{z=0} \left[ \frac{T _{z=0}}{T_{STP}} \frac{P_{STP}}{P} \right]$	$\frac{\partial(Feed)}{\partial t} = 0$	$\frac{\partial(Feed)}{\partial t} = 0$

$\frac{\partial(\text{Product}_i)}{\partial t} = 0$	$\frac{\partial(\text{Product}_i)}{\partial t} = \frac{uP_i}{RT} \Big _{z=L} \left[ \frac{T _{z=L} P_{STP}}{T_{STP} P} \right]$	$\frac{\partial(\text{Product}_i)}{\partial t} = 0$	$\frac{\partial(\text{Product}_i)}{\partial t} = 0$
$\frac{\partial(\text{Exhaust}_i)}{\partial t} = 0$	$\frac{\partial(\text{Exhaust}_i)}{\partial t} = 0$	$\frac{\partial(\text{Exhaust})}{\partial t} = -\frac{uP_i}{RT} \Big _{z=0} \left[ \frac{T _{z=0} P_{STP}}{T_{STP} P} \right]$	$\frac{\partial(\text{Exhaust})}{\partial t} = -\frac{uP_i}{RT} \Big _{z=0} \left[ \frac{T _{z=0} P_{STP}}{T_{STP} P} \right]$
$\frac{\partial(\text{PurgeFeed}_i)}{\partial t} = 0$	$\frac{\partial(\text{PurgeFeed}_i)}{\partial t} = 0$	$\frac{\partial(\text{PurgeFeed}_i)}{\partial t} = 0$	$\frac{\partial(\text{PurgeFeed}_i)}{\partial t} = -\frac{uP_i}{RT} \Big _{z=L} \left[ \frac{T _{z=L} P_{STP}}{T_{STP} P} \right]$

**Table 4-2. Mole flux variables at each operating step of FVPSA**

Pressurization	Adsorption	Cocurrent blowdown	Countercurrent regeneration
$\frac{\partial(Feed_i)}{\partial t}$ $= \frac{uP_i}{RT} \Big _{z=0} \left[ \frac{T _{z=0}}{T_{STP}} \frac{P_{STP}}{P} \right]$	$\frac{\partial(Feed_i)}{\partial t}$ $= \frac{uP_i}{RT} \Big _{z=0} \left[ \frac{T _{z=0}}{T_{STP}} \frac{P_{STP}}{P} \right]$	$\frac{\partial(Feed)}{\partial t} = 0$	$\frac{\partial(Feed)}{\partial t} = 0$
$\frac{\partial(Product_i)}{\partial t} = 0$	$\frac{\partial(Product_i)}{\partial t}$ $= \frac{uP_i}{RT} \Big _{z=L} \left[ \frac{T _{z=L}}{T_{STP}} \frac{P_{STP}}{P} \right]$	$\frac{\partial(Product_i)}{\partial t}$ $= \frac{uP_i}{RT} \Big _{z=L} \left[ \frac{T _{z=L}}{T_{STP}} \frac{P_{STP}}{P} \right]$	$\frac{\partial(Product_i)}{\partial t} = 0$
$\frac{\partial(Exhaust_i)}{\partial t} = 0$	$\frac{\partial(Exhaust_i)}{\partial t} = 0$	$\frac{\partial(Exhaust_i)}{\partial t} = 0$	$\frac{\partial(Exhaust)}{\partial t}$ $= - \frac{uP_i}{RT} \Big _{z=0} \left[ \frac{T _{z=0}}{T_{STP}} \frac{P_{STP}}{P} \right]$
$\frac{\partial(PurgeFeed_i)}{\partial t} = 0$	$\frac{\partial(PurgeFeed_i)}{\partial t} = 0$	$\frac{\partial(PurgeFeed_i)}{\partial t} = 0$	$\frac{\partial(PurgeFeed_i)}{\partial t} = 0$

**Table 5-1. Boundary conditions of PSA operation**

Pressurization	Adsorption	Depressurization	Regeneration
$y_i _{z=0} = y_{f,i}$	$y_i _{z=0} = y_{f,i}$	$\frac{\partial y_i}{\partial z} \Big _{z=0} = 0$	$\frac{\partial y_i}{\partial z} \Big _{z=0} = 0$
$\frac{\partial y_i}{\partial z} \Big _{z=L} = 0$	$\frac{\partial y_i}{\partial z} \Big _{z=L} = 0$	$\frac{\partial y_i}{\partial z} \Big _{z=L} = 0$	$y_{CO_2} _{z=L} = 0; y_{N_2} _{z=L} = 1$
$T _{z=0} = T_{feed}$	$T _{z=0} = T_{feed}$	$\frac{\partial T}{\partial z} \Big _{z=0} = 0$	$\frac{\partial T}{\partial z} \Big _{z=0} = 0$
$\frac{\partial T}{\partial z} \Big _{z=L} = 0$	$\frac{\partial T}{\partial z} \Big _{z=L} = 0$	$\frac{\partial T}{\partial z} \Big _{z=L} = 0$	$T _{z=L} = T_{purge}$
$u _{z=0} \Leftarrow eq.(8)$	$u _{z=0} = u_{feed}$	$u _{z=0} \Leftarrow eq.(8)$	$u _{z=0} \Leftarrow eq.(4)$
$u _{z=L} = 0$	$u _{z=L} \Leftarrow eq.(4)$	$u _{z=L} = 0$	$u _{z=L} = u_{purge}$

**Table 5-2. Boundary conditions of FVPSA operation**

Pressurization	Adsorption	Cocurrent blowdown	Countercurrent regeneration
$y_i _{z=0} = y_{f,i}$	$y_i _{z=0} = y_{f,i}$	$\frac{\partial y_i}{\partial z} _{z=0} = 0$	$\frac{\partial y_i}{\partial z} _{z=0} = 0$
$\frac{\partial y_i}{\partial z} _{z=L} = 0$			
$T _{z=0} = T_{feed}$	$T _{z=0} = T_{feed}$	$\frac{\partial T}{\partial z} _{z=0} = 0$	$\frac{\partial T}{\partial z} _{z=0} = 0$
$\frac{\partial T}{\partial z} _{z=L} = 0$			
$u _{z=0} \Leftarrow eq.(8)$	$u _{z=0} = u_{feed}$	$u _{z=0} = 0$	$u _{z=0} \Leftarrow eq.(8)$
$u _{z=L} = 0$	$u _{z=L} \Leftarrow eq.(4)$	$u _{z=L} \Leftarrow eq.(8)$	$u _{z=L} = 0$

The resulting mathematical model consists of a set of partial differential and algebraic equations that is solved using the gPROMS modeling tool [20, 21]. The centered finite difference method (CFDM) is used to discretize the spatial domains. The reduced space SQP algorithm is adopted for the optimization.

### 3. Optimization Strategies

**3.1. Cyclic steady state (CSS).** CSS should be determined for the optimization of cyclic adsorption processes and the definition of CSS is that the bed profiles at the beginning of the cycle are the same as those at the end of the cycle. So the initial conditions are determined by this CSS definition given by:

$$\phi|_{t=0} = \phi|_{t=cycle} \quad \text{where } \phi = y_i, q_i, T \quad \text{for } 0 < z < L, \quad \text{and } q_i(0), q_i(L) \quad (19)$$

For the CSS profile expression, our previous optimization approach, tailored single discretization (TSD), employed the following type of function to define the initial condition[3]:

$$\phi|_{t=0} = f(z), \quad \text{here } f(z) = k_a + \frac{k_b}{1 + \exp\left(-\frac{z - k_c}{k_d}\right)} \quad (20)$$

The function type ( $f(z)$ ) may be changed depending on the CSS shape. That is to say, the function type with initial values of the parameters ( $k_a$ ,  $k_b$ ,  $k_c$ , and  $k_d$ ) is obtained from a nonlinear regression based on successive substitution (SS) from the first cycle to CSS cycle ( $\approx 500^{\text{th}}$  cycle or  $1,000^{\text{th}}$  cycle). The parameters ( $k_a$ ,  $k_b$ ,  $k_c$ , and  $k_d$ ) at CSS are decided from the optimization to satisfy the following modified CSS conditions (equation 21) instead of equation (19)[3].

$$\left| \left[ \int \phi dz \right]_{t=0} - \left[ \int \phi dz \right]_{t=t_{\text{cycle}}} \right| \leq \delta, \text{ where } \delta \text{ is a small positive constant} \quad (21)$$

In the updated TSD (uTSD) approach, the following is used for the CSS determination as in the work by Jiang et al. [22]

$$-\varepsilon \leq [\phi]_{t=0,n} - [\phi]_{t=t_{\text{cycle}},n} \leq \varepsilon, \quad (22)$$

where,

$\varepsilon$  is a nonnegative variable which is minimized during the optimization;

$n$  is an axial point at each node of the finite difference or finite element method.

In the TSD and uTSD methods, the CSS condition is decided by the optimization. The previous method obtains the CSS by using the CSS constraint (equation 21) with the small CSS tolerance ( $\square$ ), and the new method determines this by minimizing the CSS variable ( $\varepsilon$ ) in the CSS constraint (equation 22).

**3.2. Optimization algorithms.** We briefly compare the new optimization method with the TSD method developed in [2, 3]. In this study we propose a new uTSD approach, which adopts the same discretization concept as TSD. Like TSD it uses binary variables to express the changing operating conditions and update the optimization procedure.

The tailored single discretization (TSD) optimization strategy is summarized below [2, 3]:

- 1) Formulation of the model by using single discretization (SD) approach.
- 2) Expression of the operating step changes for the PSA operation by using binary variables.
- 3) CSS prediction with regression.
  - (1) Obtain the approximate CSS profile through successive substitution (SS) from 1st cycle to CSS cycle ( $\approx$ 500th or 1000th cycle)
  - (2) Guess functions (equation 17) which express the CSS profile from a parameter regression
- 4) Addition of the CSS constraints (equation 18) to the optimization model as the inequality constraint with the small positive tolerance ( $\square$ ).
- 5) Optimization of the PSA model with the CSS constraints by minimizing the objective function ( $\Phi$ ).

This approach has advantages over the complete discretization (CD) method in cyclic adsorption process optimization, but this has the two shortcomings:

- The CSS condition is only approximate. It is obtained by setting the small tolerance; however, sometimes this very small tolerance makes it difficult to converge to the optimal point or requires a long computation time for the optimization.
- A nonlinear regression step is required to get the proper function describing the CSS profile accurately; however, the regression may sometimes be impossible or inaccurate when the real CSS shape is not predictable by any function type.

To eliminate the above problems, this work proposes the following uTSD approach, which removes the regression step from the optimization procedure and determines the CSS profiles by minimizing  $\Phi$ .

- 1) Formulation of the model by using single discretization (SD) approach.
- 2) Expression of the operating step changes for the PSA operation by using binary variables.
- 3) CSS prediction: Successive substitution (SS) from 1st cycle to CSS to get the initial values of  $\phi$  at each node for the CSS optimization.
- 4) Addition of the CSS constraints (equation 19), with the nonnegative variable ( $\epsilon$ ) applied at each axial point at CSS.

Optimization of the PSA model with the CSS constraints by minimizing the objective function ( $\Phi$ ) as well as the nonnegative variable ( $\epsilon$ ), i.e.,  $Min \Phi + M\epsilon$ , where  $M$  is a large value ( $\approx 10^5$ ).

## 4. Optimization Results

### 4.1. Comparison of the new TSD and the previous TSD.

To demonstrate that the new method is better than the previous one, this study first considers a simplified PSA process. The model is not as detailed as the current target processes (normal temperature PSA, high temperature PSA and FVPSA of this work), but allows us to compare the methods easily and quickly. The operation is the Skarstrom cycle shown in the Figure 3.

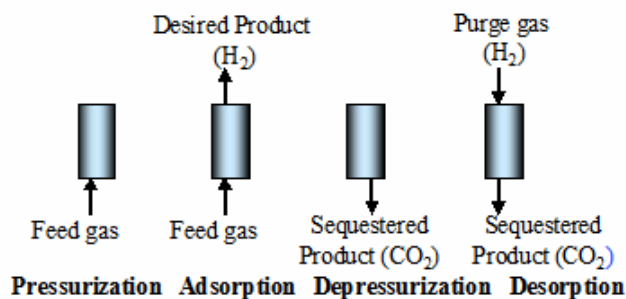


Figure 3. H<sub>2</sub>/CO<sub>2</sub> gas separation PSA process

The optimization formulation is

$$\text{Min. Power/Purity}_{\text{H}_2} \quad \text{for TSD} \quad (23-1)$$

$$\text{Min. Power/Purity}_{\text{H}_2} + M\varepsilon \text{ for uTSD} \quad (23-2)$$

s.t.

$$0.3\text{m} \leq L \leq 3\text{m} \quad (24a)$$

$$3\text{atm} \leq P_{\text{feed}} \leq 20\text{atm} \quad (24b)$$

$$1\text{sec} \leq t_P, t_{\text{DP}} \leq 50\text{sec} \quad (24c)$$

$$80\text{sec} \leq t_A, t_R \leq 950\text{sec} \quad (24d)$$

$$0.004\text{m/sec} \leq u_{\text{feed}} \leq 0.1\text{m/sec} \quad (24e)$$

$$-0.2\text{m/sec} \leq u_{\text{purge}} \leq -4\text{E-}5\text{m/sec} \quad (24f)$$

$$0.9 \leq \text{Purity}_{\text{H}_2} \leq 1 \quad (24g)$$

$$\text{Power} \leq 40 \quad (24h)$$

General PSA model equations [23]

Judging from the optimization results in Table 6, the updated tailored single discretization (uTSD) has the following advantages over the tailored single discretization (TSD): fewer iterations, faster calculation, more accurate CSS ( $\varepsilon = 1.29858 \times 10^{-24} \approx 0$ ), and better results.

**Table 6. Optimization results of the previous TSD and updated TSD**

Optimization algorithm by Ko et al.	Previous TSD	updated TSD
Total CPU Time for Optimization	1,667.03 sec	628.265 sec
No. of NLP Iterations	66	32
No. of Line Search Steps	145	34
Purity <sub>H2</sub>	95.1694%	95.1458%
Power	6.13834 W	2.9283 W
CSS accuracy ( $\int_0^L  q_{1,t=0} - q_{1,t=t_{\text{cycle}}}  dz$ )	0.02995	$5.19391 \times 10^{-8}$
CSS accuracy ( $\int_0^L  q_{2,t=0} - q_{2,t=t_{\text{cycle}}}  dz$ )	0.02601	$1.33813 \times 10^{-8}$
CSS accuracy ( $\int_0^L  y_{i,t=0} - y_{i,t=t_{\text{cycle}}}  dz$ )	0.03012	$1.02731 \times 10^{-7}$
Objective function value	0.0451494	0.0215438
Here, the optimal value of $\varepsilon$ in uTSD is $1.29858 \times 10^{-24}$		

## 4.2. PSA Optimization at normal temperature region

Two optimization cases for CO<sub>2</sub> sequestration are presented in this section. The following is the optimization model:

$$\text{Min. } Objective = -Purity_{CO_2} - Purity_{N_2} + M\varepsilon \quad (25)$$

Subject to

$$10 \text{ sec} \leq t_p \leq 50 \text{ sec} \quad (26-1)$$

$$35 \text{ sec} \leq t_A \leq 115 \text{ sec} \quad (26-2)$$

$$10 \text{ sec} \leq t_{DP} \leq 60 \text{ sec} \quad (26-3)$$

$$35 \text{ sec} \leq t_R \leq 105 \text{ sec} \quad (26-4)$$

$$0.25 \text{ m} \leq L \leq 2 \text{ m} \quad (26-5)$$

$$170 \text{ kPa} \leq P_{feed} \leq 2,000 \text{ kPa} \quad (26-6)$$

$$90 \text{ kPa} \leq P_{initial}, P_{purge} \leq 110 \text{ kPa} \quad (26-7)$$

$$5 \text{ kPa} / \text{sec} \leq \partial P / \partial t|_{step1} \leq 50 \text{ kPa} / \text{sec} \quad (26-8)$$

$$-10^{-10} \text{ Pa} / \text{sec} \leq \partial P / \partial t|_{step2}, \partial P / \partial t|_{step4} \leq 10^{-10} \text{ Pa} / \text{sec} \quad (26-9)$$

$$-50 \text{ kPa} / \text{sec} \leq \partial P / \partial t|_{step3} \leq -2 \text{ kPa} / \text{sec} \quad (26-10)$$

$$295 \text{ K} \leq T_{feed}, T_{purge} \leq 323.15 \text{ K} \quad (26-11)$$

$$u_{ads,t=0} = 0 \quad (26-12)$$

$$10^{-5} \text{ m} / \text{sec}^2 \leq \partial u_{ads} / \partial t|_{step1} \leq 0.1 \text{ m} / \text{sec}^2 \quad (26-13)$$

$$-0.1 \text{ m} / \text{sec}^2 \leq \partial u_{ads} / \partial t|_{step2}, \partial u_{ads} / \partial t|_{step3} \leq 10^{-5} \text{ m} / \text{sec}^2 \quad (26-14)$$

$$\partial u_{ads} / \partial t|_{step4} = 0 \quad (26-15)$$

$$-0.1 \text{ m} / \text{sec} \leq u_{reg,t=0} \leq -10^{-5} \text{ m} / \text{sec} \quad (26-16)$$

$$10^{-5} \text{ m} / \text{sec}^2 \leq \partial u_{reg} / \partial t|_{step1} \leq 0.05 \text{ m} / \text{sec}^2 \quad (26-17)$$

$$\partial u_{reg} / \partial t|_{step2} = \partial u_{reg} / \partial t|_{step3} = 0 \quad (26-18)$$

$$-0.0261 \text{ m} / \text{sec}^2 \leq \partial u_{reg} / \partial t|_{step4} \leq -10^{-10} \text{ m} / \text{sec}^2 \quad (26-19)$$

$$\phi_z|_{LB} \leq \phi_z|_{t=0} \leq \phi_z|_{UB} \quad (26-20)$$

where  $\phi = q, y, \text{ or } T$

$$0 \leq z \leq \text{Length for } q_{i,z} \Big|_{t=0}$$

$$0 < z < \text{Length for } y_{i,z} \Big|_{t=0} \text{ and } T_z \Big|_{t=0}$$

$LB = \text{Lower Bound}, UB = \text{Upper Bound}$

$$0 \leq \varepsilon \leq 10^{-3} \quad (26-21)$$

$$-\varepsilon \leq \phi_z \Big|_{t=0} - \phi_z \Big|_{t=t_{\text{cycle}}} \leq \varepsilon \quad (26-22)$$

$$3 \times 10^{-9} \leq C_{v,1L} \leq 5 \times 10^{-3} \quad (26-23)$$

$$5 \times 10^{-9} \leq C_{v,3L} \leq 5 \times 10^{-2} \quad (26-24)$$

$$\text{Power}_{\text{Ave}} \leq 100 \text{ J/sec} \quad (26-25)$$

$$\text{Case A1: Purity}_{\text{CO}_2, \text{Ave}} \geq 15\% \quad (26-26a)$$

$$\text{Purity}_{\text{N}_2, \text{Ave}} \geq 85\% \quad (26-27a)$$

$$\text{Recovery}_{\text{CO}_2, \text{Ave}} \geq 15\% \quad (26-28a)$$

$$\text{Recovery}_{\text{N}_2, \text{Ave}} \geq 85\% \quad (26-29a)$$

$$\text{Case A2: Purity}_{\text{CO}_2, \text{Ave}} \geq 44\% \quad (26-26b)$$

$$\text{Purity}_{\text{N}_2, \text{Ave}} \geq 97\% \quad (26-27b)$$

$$\text{Recovery}_{\text{CO}_2, \text{Ave}} \geq 99\% \quad (26-28b)$$

$$\text{Recovery}_{\text{N}_2, \text{Ave}} \geq 86\% \quad (26-29b)$$

Equations (1)~(18), (22)

The decision variables of the PSA optimizations are the following: step times; bed length; initial bed pressure; feed pressure; pressure change rate according to the time during pressurization and depressurization step; purge pressure; temperatures; input feed gas velocity during the adsorption step; input purge gas velocity during the purge step; CSS variable ( $\varepsilon$ ); valve coefficients during pressurization and depressurization. Tables 7-1 and 7-2 list the optimization results.

**Table 7-1. Optimization results of case A1 in PSA at normal temperature region**

<i>Variables</i>	<i>Results</i>
Bed length (L)	0.319231 m
Feed pressure ( $P_{\text{feed}}$ )	718.029 kPa
Purge pressure ( $P_{\text{purge}}$ )	90.0 kPa
Initial pressure within the bed ( $P_{\text{initial}}$ )	90.0 kPa
Feed temperature ( $T_{\text{feed}}$ )	323.15 K
Purge temperature ( $T_{\text{purge}}$ )	323.15 K
Input velocity at adsorption step ( $u_{\text{feed}}$ ): Linear change of velocity at the feed end	$5.6363 \times 10^{-2}$ $\sim 4.16752 \times 10^{-2}$ m/sec
Input velocity at purge step ( $u_{\text{purge}}$ ): Linear change of velocity at the product end	$-1.59453 \times 10^{-12}$ $\sim -0.2$ m/sec
Pressurization time ( $t_P$ )	20.8985 sec
Adsorption time ( $t_A$ )	115 sec
Depressurization time ( $t_{DP}$ )	60 sec
Regeneration time ( $t_R$ )	35.035 sec
Valve coefficient at step1 ( $C_{V1L}$ )	$4.41413 \times 10^{-8}$
Valve coefficient at step3 ( $C_{V3L}$ )	$5 \times 10^{-9}$
CSS tolerance ( $\epsilon$ )	0
Average CO <sub>2</sub> purity ( $\text{Purity}_{\text{CO}_2, \text{ave}}$ )	47.7662 %
Average CO <sub>2</sub> recovery ( $\text{Recovery}_{\text{CO}_2, \text{ave}}$ )	99.9992 %
Average N <sub>2</sub> purity ( $\text{Purity}_{\text{N}_2, \text{ave}}$ )	95.2574 %
Average N <sub>2</sub> recovery ( $\text{Recovery}_{\text{N}_2, \text{ave}}$ )	85 %
Average Power at feed step ( $\text{Power}_{\text{ave}}$ )	32.1722 W
Average Specific Power at feed step ( $\text{SpecificPower}_{\text{ave}}$ )	7,112.25 W
Objective Function	143.024 %

Total CPU time = 4,222.92 sec on Pentium ® 4 with 1.8 GHz machine

Number of NLP iterations = 157

Number of NLP line search steps = 167

Optimization tolerance of NLP solver (SRQPD) = 0.001

**Table 7-2. Optimization results of case A2 in PSA at normal temperature region**

<i>Variables</i>	<i>Results</i>
Bed length (L)	0.25002 m
Feed pressure ( $P_{\text{feed}}$ )	655.358 kPa
Purge pressure ( $P_{\text{purge}}$ )	90.0 kPa
Initial pressure within the bed ( $P_{\text{initial}}$ )	90.0 kPa
Feed temperature ( $T_{\text{feed}}$ )	323.15 K
Purge temperature ( $T_{\text{purge}}$ )	323.15 K
Input velocity at adsorption step ( $u_{\text{feed}}$ ): Linear change of velocity at the feed end	$5.34327 \times 10^{-2}$ $\sim 1.6566 \times 10^{-2}$ m/sec
Input velocity at purge step ( $u_{\text{purge}}$ ): Linear change of velocity at the product end	$-1.98728 \times 10^{-7}$ $\sim -0.193841$ m/sec
Pressurization time ( $t_P$ )	21.8376 sec
Adsorption time ( $t_A$ )	115 sec
Depressurization time ( $t_{DP}$ )	59.711 sec
Regeneration time ( $t_R$ )	35 sec
Valve coefficient at step1 ( $C_{V1L}$ )	$3.26987 \times 10^{-8}$
Valve coefficient at step3 ( $C_{V3U}$ )	$5 \times 10^{-9}$
CSS tolerance ( $\epsilon$ )	0
Average CO <sub>2</sub> purity ( $\text{Purity}_{\text{CO}_2, \text{ave}}$ )	44.9549 %
Average CO <sub>2</sub> recovery ( $\text{Recovery}_{\text{CO}_2, \text{ave}}$ )	100 %
Average N <sub>2</sub> purity ( $\text{Purity}_{\text{N}_2, \text{ave}}$ )	97.0 %
Average N <sub>2</sub> recovery ( $\text{Recovery}_{\text{N}_2, \text{ave}}$ )	86.0 %
Average Power at feed step ( $\text{Power}_{\text{ave}}$ )	19.6391 W
Average Specific Power at feed step ( $\text{SpecificPower}_{\text{ave}}$ )	6,686.87 W
Objective Function	141.9549 %

Total CPU time = 1,310.34 sec on Pentium ® 4 with 1.8 GHz machine

Number of NLP iterations = 44

Number of NLP line search steps = 50

Optimization tolerance of NLP solver (SRQPD) = 0.001

### 4.3. PSA Optimization at high temperature region

Two high temperature PSA models for CO<sub>2</sub> sequestration are also performed. The optimization models and the decision variables are the same as the models in section 4.2, except with the following differences in step times, temperature, gas velocities and product specification:

Subject to

$$10 \text{ sec} \leq t_p \leq 50 \text{ sec} \quad (27-1)$$

$$35 \text{ sec} \leq t_A \leq 145 \text{ sec} \quad (27-2)$$

$$10 \text{ sec} \leq t_{DP} \leq 80 \text{ sec} \quad (27-3)$$

$$20 \text{ sec} \leq t_R \leq 105 \text{ sec} \quad (27-4)$$

$$295 \text{ K} \leq T_{\text{feed}}, T_{\text{purge}} \leq 370.15 \text{ K} \quad (27-5)$$

$$-10^{-5} \text{ m/sec} \leq u_{\text{ads}, t=0} \leq 0.11 \text{ m/sec} \quad (27-6)$$

$$-0.12 \text{ m/sec} \leq u_{\text{reg}, t=0} \leq -10^{-5} \text{ m/sec} \quad (27-7)$$

$$3 \times 10^{-9} \leq C_{v,1L} \leq 5 \times 10^{-3} \quad (27-8)$$

$$4 \times 10^{-9} \leq C_{v,3L} \leq 5 \times 10^{-2} \quad (27-9)$$

$$\text{Case B1: } Purity_{CO_2, Ave} \geq 47\% \quad (27-10a)$$

$$Purity_{N_2, Ave} \geq 97\% \quad (27-11a)$$

$$Recovery_{CO_2, Ave} \geq 15\% \quad (27-12a)$$

$$Recovery_{N_2, Ave} \geq 85\% \quad (27-13a)$$

$$\text{Case B2: } Purity_{CO_2, Ave} \geq 53\% \quad (27-10b)$$

$$Purity_{N_2, Ave} \geq 98\% \quad (27-11b)$$

$$Recovery_{CO_2, Ave} \geq 99\% \quad (27-12b)$$

$$Recovery_{N_2, Ave} \geq 86\% \quad (27-13b)$$

Tables 8-1 and 8-2 summarize the optimization results.

**Table 8-1. Optimization results of case B1 in PSA at high temperature region**

<i>Variables</i>	<i>Results</i>
Bed length (L)	0.344343 m
Feed pressure ( $P_{\text{feed}}$ )	784.174 kPa
Purge pressure ( $P_{\text{purge}}$ )	90.000 kPa
Initial pressure within the bed ( $P_{\text{initial}}$ )	90.000 kPa
Feed temperature ( $T_{\text{feed}}$ )	370.15 K
Purge temperature ( $T_{\text{purge}}$ )	370.15 K
Input velocity at adsorption step ( $u_{\text{feed}}$ ): Linear change of velocity at the feed end	$3.90816 \times 10^{-2}$ $\sim 1.61418 \times 10^{-2}$ m/sec
Input velocity at purge step ( $u_{\text{purge}}$ ): Linear change of velocity at the product end	$-2.1525 \times 10^{-8}$ $\sim -0.12$ m/sec
Pressurization time ( $t_P$ )	41.1225 sec
Adsorption time ( $t_A$ )	145 sec
Depressurization time ( $t_{DP}$ )	78.5842 sec
Regeneration time ( $t_R$ )	32.5934 sec
Valve coefficient at step1 ( $C_{V1L}$ )	$1.3704 \times 10^{-8}$
Valve coefficient at step3 ( $C_{V3L}$ )	$4 \times 10^{-9}$
CSS tolerance ( $\epsilon$ )	$-4.7414 \times 10^{-21}$
Average CO <sub>2</sub> purity ( $\text{Purity}_{\text{CO}_2, \text{ave}}$ )	59.3687 %
Average CO <sub>2</sub> recovery ( $\text{Recovery}_{\text{CO}_2, \text{ave}}$ )	100.0 %
Average N <sub>2</sub> purity ( $\text{Purity}_{\text{N}_2, \text{ave}}$ )	97.0 %
Average N <sub>2</sub> recovery ( $\text{Recovery}_{\text{N}_2, \text{ave}}$ )	85.0785 %
Average Power at feed step ( $\text{Power}_{\text{ave}}$ )	19.2355 W
Average Specific Power at feed step ( $\text{SpecificPower}_{\text{ave}}$ )	8,629.03 W
Objective Function	156.369 %

Total CPU time = 5,394.53 sec on Pentium ® 4 with 1.8 GHz machine

Number of NLP iterations = 208

Number of NLP line search steps = 238

Optimization tolerance of NLP solver (SRQPD) = 0.001

**Table 8-2. Optimization results of case B2 in PSA at high temperature region**

<i>Variables</i>	<i>Results</i>
Bed length (L)	0.267065 m
Feed pressure ( $P_{\text{feed}}$ )	709.942 kPa
Purge pressure ( $P_{\text{purge}}$ )	90.00 kPa
Initial pressure within the bed ( $P_{\text{initial}}$ )	90.00 kPa
Feed temperature ( $T_{\text{feed}}$ )	370.15 K
Purge temperature ( $T_{\text{purge}}$ )	370.15 K
Input velocity at adsorption step ( $u_{\text{feed}}$ ): Linear change of velocity at the feed end	$4.80913 \times 10^{-2}$ $\sim 1.36809 \times 10^{-3}$ m/sec
Input velocity at purge step ( $u_{\text{purge}}$ ): Linear change of velocity at the product end	$-1.51995 \times 10^{-7}$ $\sim -0.12$ m/sec
Pressurization time ( $t_P$ )	42.9705 sec
Adsorption time ( $t_A$ )	145 sec
Depressurization time ( $t_{DP}$ )	76.5696 sec
Regeneration time ( $t_R$ )	39.338 sec
Valve coefficient at step1 ( $C_{V1L}$ )	$1.48999 \times 10^{-8}$
Valve coefficient at step3 ( $C_{V3U}$ )	$4 \times 10^{-9}$
CSS tolerance ( $\epsilon$ )	0
Average CO <sub>2</sub> purity ( $\text{Purity}_{\text{CO}_2, \text{ave}}$ )	55.7042 %
Average CO <sub>2</sub> recovery ( $\text{Recovery}_{\text{CO}_2, \text{ave}}$ )	100 %
Average N <sub>2</sub> purity ( $\text{Purity}_{\text{N}_2, \text{ave}}$ )	98.00 %
Average N <sub>2</sub> recovery ( $\text{Recovery}_{\text{N}_2, \text{ave}}$ )	86.0004 %
Average Power at feed step ( $\text{Power}_{\text{ave}}$ )	14.6806 J/sec
Average Specific Power at feed step ( $\text{SpecificPower}_{\text{ave}}$ )	8,085.56 W
Objective Function	153.7042 %

Total CPU time = 3,451.22 sec on Pentium ® 4 with 1.8 GHz machine

Number of NLP iterations = 129

Number of NLP line search steps = 138

Optimization tolerance of NLP solver (SRQPD) = 0.001

#### 4.4. FVPSA Optimization at high temperature region

To improve the purities over PSA, the three FVPSA processes are optimized. The optimization results are listed in Table 8, and the optimization formulation is given by:

$$\text{Min. Objective} = -\text{Purity}_{CO_2} - \text{Purity}_{N_2} + M\varepsilon \quad (28)$$

Subject to

$$10\text{sec} \leq t_p \leq 55\text{sec} \quad (29-1)$$

$$35\text{sec} \leq t_A \leq 150\text{sec} \quad (29-2)$$

$$10\text{sec} \leq t_{PRO} \leq 55\text{sec} \quad \text{for case C1} \quad (29-3a)$$

$$10\text{sec} \leq t_{PRO} \leq 60\text{sec} \quad \text{for cases C2 and C3} \quad (29-3b,c)$$

$$35\text{sec} \leq t_R \leq 150\text{sec} \quad (29-4)$$

$$0.25\text{m} \leq \text{Length} \leq 2\text{m} \quad (29-5)$$

$$170\text{kPa} \leq P_{feed} \leq 2,000\text{kPa} \quad (29-6)$$

$$70\text{kPa} \leq P_{pro} \leq 130\text{kPa} \quad (29-7)$$

$$9.9\text{kPa} \leq P_{reg}, P_{initial} \leq 70\text{kPa} \quad (29-8)$$

$$5.0\text{kPa} / \text{sec} \leq \partial P / \partial t|_{step1} \leq 50\text{kPa} / \text{sec} \quad (29-9)$$

$$-10^{-10} \text{Pa} / \text{sec} \leq \partial P / \partial t|_{step2} \leq 10^{-10} \text{Pa} / \text{sec} \quad (29-10)$$

$$-50.0\text{kPa} / \text{sec} \leq \partial P / \partial t|_{step3} \leq -2.0\text{Pa} / \text{sec} \quad (29-11)$$

$$-9.0\text{kPa} / \text{sec} \leq \partial P / \partial t|_{step4} \leq -0.100\text{kPa} / \text{sec} \quad (29-12)$$

$$275\text{K} \leq T_{feed} \leq 370\text{K} \quad (29-13)$$

$$u_{ads,t=0} = 0 \quad (29-14)$$

$$10^{-5} \text{m} / \text{sec}^2 \leq \partial u_{ads} / \partial t|_{step1} \leq 0.1\text{m} / \text{sec}^2 \quad (29-15)$$

$$-0.1\text{m} / \text{sec}^2 \leq \partial u_{ads} / \partial t|_{step2} \leq 3 \times 10^{-3} \text{m} / \text{sec}^2 \quad (29-16)$$

$$-0.1\text{m} / \text{sec}^2 \leq \partial u_{ads} / \partial t|_{step3} \leq 10^{-5} \text{m} / \text{sec}^2 \quad (29-17)$$

$$\partial u_{ads} / \partial t|_{step4} = 0 \quad (29-18)$$

$$\phi_z|_{LB} \leq \phi_z|_{t=0} \leq \phi_z|_{UB} \quad (29-19)$$

where  $\phi = q, y, \text{ or } T$

$$0 \leq z \leq \text{Length for } q_{i,z}|_{t=0}$$

$$0 < z < \text{Length for } y_{i,z} \Big|_{t=0} \text{ and } T_z \Big|_{t=0}$$

*LB = Lower Bound, UB = Upper Bound*

$$0 \leq \varepsilon \leq 10^{-3} \quad (29-20)$$

$$-\varepsilon \leq \phi_z \Big|_{t=0} - \phi_z \Big|_{t=t_{\text{cycle}}} \leq \varepsilon \quad (29-21)$$

$$5 \times 10^{-9} \leq C_{v,1L} \leq 5 \times 10^{-3} \quad (29-22)$$

$$5 \times 10^{-9} \leq C_{v,3U} \leq 5 \times 10^{-2} \quad (29-23)$$

$$5 \times 10^{-9} \leq C_{v,4L} \leq 5 \times 10^{-3} \quad (29-24)$$

$$\text{Case C1: Purity}_{CO_2, Ave} \geq 82\% \quad (29-25a)$$

$$\text{Purity}_{N_2, Ave} \geq 97\% \quad (29-26a)$$

$$\text{Recovery}_{CO_2, Ave} \geq 15\% \quad (29-27a)$$

$$\text{Recovery}_{N_2, Ave} \geq 85\% \quad (29-28a)$$

$$\text{Power}_{Ave} \leq 500,000 J / \text{sec} \quad (29-29a)$$

$$\text{Case C2: Purity}_{CO_2, Ave} \geq 90\% \quad (29-25b)$$

$$\text{Purity}_{N_2, Ave} \geq 99\% \quad (29-26b)$$

$$\text{Recovery}_{CO_2, Ave} \geq 80\% \quad (29-27b)$$

$$\text{Recovery}_{N_2, Ave} \geq 90\% \quad (29-28b)$$

$$\text{Power}_{Ave} \leq 700,000 W \quad (29-29b)$$

$$\text{Case C3: Purity}_{CO_2, Ave} \geq 90\% \quad (29-25c)$$

$$\text{Purity}_{N_2, Ave} \geq 99\% \quad (29-26c)$$

$$\text{Recovery}_{CO_2, Ave} \geq 95\% \quad (29-27c)$$

$$\text{Recovery}_{N_2, Ave} \geq 95\% \quad (29-28c)$$

$$\text{Power}_{Ave} \leq 700,000 W \quad (29-29c)$$

The decision variables of the FVPSA optimizations are the following: step times; bed length; initial bed pressure; feed pressure; product purge pressure; regeneration pressure; pressure change rate according to the time during the pressurization, product purge and regeneration steps; temperatures; input feed gas velocity during the adsorption step; the CSS tolerance ( $\varepsilon$ ); valve coefficients during the pressurization, product purge and regeneration steps. Tables 9-1, 9-2 and 9-3 list the optimization results.

**Table 9-1. Optimization results of case C1 in FVPSA at high temperature region**

<i>Variables</i>	<i>Results</i>
Bed length (L)	0.25 m
Feed pressure ( $P_{\text{feed}}$ )	693.482 kPa
Cocurrent blowdown product pressure ( $P_{\text{pro}}$ )	70.00 kPa
Countercurrent regeneration pressure ( $P_{\text{reg}}$ )	9.900 kPa
Initial pressure within the bed ( $P_{\text{initial}}$ )	9.900 kPa
Feed temperature ( $T_{\text{feed}}$ )	365.316 K
Input velocity at adsorption step ( $u_{\text{feed}}$ ): Linear change of velocity at the feed end	$2.29158 \times 10^{-2}$ $\sim 3.00148 \times 10^{-2}$ m/sec
Pressurization time ( $t_p$ )	47.4861 sec
Adsorption time ( $t_A$ )	132.003 sec
Cocurrent blowdown time ( $t_{\text{PRO}}$ )	54.7927 sec
Regeneration time ( $t_R$ )	35.7814 sec
Valve coefficient at step1 ( $C_{v1L}$ )	$1.03919 \times 10^{-4}$
Valve coefficient at step3 ( $C_{v3U}$ )	$8.76024 \times 10^{-4}$
Valve coefficient at step4 ( $C_{v4L}$ )	$2.4652 \times 10^{-4}$
CSS tolerance ( $\epsilon$ )	$7.62875 \times 10^{-17}$
Average CO <sub>2</sub> purity ( $\text{Purity}_{\text{CO}_2, \text{ave}}$ )	95.4624 %
Average CO <sub>2</sub> recovery ( $\text{Recovery}_{\text{CO}_2, \text{ave}}$ )	15.0002 %
Average N <sub>2</sub> purity ( $\text{Purity}_{\text{N}_2, \text{ave}}$ )	97.7535 %
Average N <sub>2</sub> recovery ( $\text{Recovery}_{\text{N}_2, \text{ave}}$ )	100. %
Average Power at feed step ( $\text{Power}_{\text{ave}}$ )	44,352.2 W
Average Specific Power at feed step ( $\text{SpecificPower}_{\text{ave}}$ )	7,855.65 W
Objective Function	193.2159 %

Total CPU time = 7,503.51 sec on Pentium ® 4 with 1.8 GHz machine

Number of NLP iterations = 100

Number of NLP line search steps = 123

Optimization tolerance of NLP solver (SRQPD) = 0.002

**Table 9-2. Optimization results of case C2 in FVPSA at high temperature region**

<i>Variables</i>	<i>Results</i>
Bed length (L)	0.388057 m
Feed pressure ( $P_{\text{feed}}$ )	869.326 kPa
Cocurrent blowdown product pressure ( $P_{\text{pro}}$ )	70.00 kPa
Countercurrent regeneration pressure ( $P_{\text{reg}}$ )	9.90 kPa
Initial pressure within the bed ( $P_{\text{initial}}$ )	9.90 kPa
Feed temperature ( $T_{\text{feed}}$ )	364.419 K
Input velocity at adsorption step ( $u_{\text{feed}}$ ): Linear change of velocity at the feed end	0.107635 ~ 0.0966774 m/sec
Pressurization time ( $t_p$ )	17.9491 sec
Adsorption time ( $t_A$ )	45.0058 sec
Cocurrent blowdown time ( $t_{\text{PRO}}$ )	59.9936 sec
Regeneration time ( $t_R$ )	55.5020 sec
Valve coefficient at step1 ( $C_{v1L}$ )	$5.65053 \times 10^{-4}$
Valve coefficient at step3 ( $C_{v3U}$ )	$4.07110 \times 10^{-5}$
Valve coefficient at step4 ( $C_{v4L}$ )	$3.68561 \times 10^{-4}$
CSS tolerance ( $\epsilon$ )	$5.89807 \times 10^{-17}$
Average CO <sub>2</sub> purity ( $\text{Purity}_{\text{CO}_2, \text{ave}}$ )	92.2936 %
Average CO <sub>2</sub> recovery ( $\text{Recovery}_{\text{CO}_2, \text{ave}}$ )	79.9985 %
Average N <sub>2</sub> purity ( $\text{Purity}_{\text{N}_2, \text{ave}}$ )	99.00 %
Average N <sub>2</sub> recovery ( $\text{Recovery}_{\text{N}_2, \text{ave}}$ )	99.9981 %
Average Power at feed step ( $\text{Power}_{\text{ave}}$ )	300,393 W
Average Specific Power at feed step ( $\text{SpecificPower}_{\text{ave}}$ )	9,066.34 W
Objective Function	191.2936 %

Total CPU time = 3,581.23 sec on Pentium ® 4 with 1.8 GHz machine

Number of NLP iterations = 77

Number of NLP line search steps = 81

Optimization tolerance of NLP solver (SRQPD) = 0.002

**Table 9-3. Optimization results of case C3 in high temperature FVPSA process**

<i>Variables</i>	<i>Results</i>
Bed length (L)	0.966855 m
Feed pressure ( $P_{\text{feed}}$ )	902.959 kPa
Cocurrent blowdown product pressure ( $P_{\text{pro}}$ )	70.00 kPa
Countercurrent regeneration pressure ( $P_{\text{reg}}$ )	9.90 kPa
Initial pressure within the bed ( $P_{\text{initial}}$ )	9.90 kPa
Feed temperature ( $T_{\text{feed}}$ )	365.373 K
Input velocity at adsorption step ( $u_{\text{feed}}$ ): Linear change of velocity at the feed end	0.215801 ~0.217474 m/sec
Pressurization time ( $t_p$ )	19.0672 sec
Adsorption time ( $t_A$ )	54.6696 sec
Cocurrent blowdown time ( $t_{\text{PRO}}$ )	59.3987 sec
Regeneration time ( $t_R$ )	57.8045 sec
Valve coefficient at step1 ( $C_{v1L}$ )	$1.1498 \times 10^{-3}$
Valve coefficient at step3 ( $C_{v3U}$ )	$9.06724 \times 10^{-5}$
Valve coefficient at step4 ( $C_{v4L}$ )	$1.09952 \times 10^{-3}$
CSS tolerance ( $\epsilon$ )	$1.2845 \times 10^{-17}$
Average CO <sub>2</sub> purity ( $\text{Purity}_{\text{CO}_2, \text{ave}}$ )	91.9232 %
Average CO <sub>2</sub> recovery ( $\text{Recovery}_{\text{CO}_2, \text{ave}}$ )	95.0012 %
Average N <sub>2</sub> purity ( $\text{Purity}_{\text{N}_2, \text{ave}}$ )	99.0321 %
Average N <sub>2</sub> recovery ( $\text{Recovery}_{\text{N}_2, \text{ave}}$ )	100 %
Average Power at feed step ( $\text{Power}_{\text{ave}}$ )	648,504 W
Average Specific Power at feed step ( $\text{SpecificPower}_{\text{ave}}$ )	9,305.14 W
Objective Function	190.9553 %

Total CPU time = 4,764.8 sec on Pentium ® 4 with 1.8 GHz machine

Number of NLP iterations = 102

Number of NLP line search steps = 128

Optimization tolerance of NLP solver (SRQPD) = 0.002

## 5. Conclusions

An improved optimization algorithm is described for PSA. The updated PSA optimization method shows the following advantages over the previous method (Ko et al., 2002 and 2003): 1) faster calculation, 2) more robust convergence, and 3) more accurate CSS. With the new optimization procedure, we performed the simulations and optimizations of the normal temperature PSA, the high temperature PSA and the FVPSA processes to get high CO<sub>2</sub> purity

as well as N<sub>2</sub> purity from the mixture gas (85% N<sub>2</sub> and 15% CO<sub>2</sub>). The process models are formulated by using partial differential algebraic equations (PDAEs) that describe the dynamic behaviors and spatial distribution of the variables within the bed. The centered finite difference method (CFDM) is used for the discretization of the spatial domain, and a reduced space SQP algorithm is adopted for the optimizations.

The optimization results lead to the following observations:

- As the PSA models are more constrained (cases A2 and B2), the optimal bed lengths become smaller. Since most adsorption occurs close to the feed end of the bed than at the product end, a longer bed does not seem to be necessary and a length of 25cm might be good enough to satisfy the tighter constraints in the PSA optimizations. However, to increase the average N<sub>2</sub> purity and CO<sub>2</sub> recovery simultaneously, a longer bed length is required in the FVPSA process.
- Average N<sub>2</sub> purities of the normal temperature PSA processes are more affected by the contact time of the adsorption step than by the feed pressure of the step. That is, the higher N<sub>2</sub> purity is obtained by the larger contact time in normal temperature PSA processes. In high temperature PSA, the larger contact time and higher feed pressure may lead to lower N<sub>2</sub> purity. On the other hand, for FVPSA the effect of feed pressure on N<sub>2</sub> purity is stronger than that of contact time. So the N<sub>2</sub> purity can be improved by increasing the feed pressure in the FVPSA processes.
- The optimal purge and blowdown pressures are almost at the lower bounds of the optimization constraints. This means that the regeneration of CO<sub>2</sub> can be improved by reducing the pressure at the regeneration (purge) step. The cocurrent blowdown step of FVPSA to evacuate the N<sub>2</sub> within the bed also requires the low pressure (lower bound), so that the average N<sub>2</sub> recovery can be 100% in FVPSA processes.
- In PSA, the optimized adsorption times are the upper bounds of optimization constraints because the average N<sub>2</sub> recovery increases and the increasing rate becomes smaller over time. The optimal regeneration time of PSA is small because the average CO<sub>2</sub> purity quickly increases and then starts decreasing as the regeneration proceeds. In FVPSA, we note that average CO<sub>2</sub> recovery increases with regeneration time. CO<sub>2</sub> purity decreases accordingly as CO<sub>2</sub> recovery increases.
- The adsorption times of Cases C2 and C3 (FVPSA to get 99% of N<sub>2</sub> purities) are shorter than the adsorption time of Case C1 (FVPSA to get 97% purity) because N<sub>2</sub> purity decreases slightly as the adsorption and cocurrent blowdown steps proceed.
- The optimal gas velocity for FVPSA processes is much larger than for PSA processes. For high CO<sub>2</sub> purity more CO<sub>2</sub> is adsorbed and regenerated. Also, the optimal values of valve coefficients in FVPSA are much larger than those in PSA.

In summary, we can conclude that 1) FVPSA is much better than PSA in obtaining high purities of CO<sub>2</sub> (about 92%~95%) and N<sub>2</sub> (about 99%), 2) CO<sub>2</sub> recoveries of FVPSA is low (about 15%~95%), compared with those of PSA (almost 100%), 3) N<sub>2</sub> purities of high temperature processes can also be higher (98%) than those of normal temperature PSA (97%), 4) N<sub>2</sub> recoveries of FVPSA are almost 100% and those of PSA are 85 % or a little higher, and 5) the average power (watts) for FVPSA operation is much larger than that for PSA operation because the input gas velocity and valve coefficient value of FVPSA is much bigger than those of PSA. On the other hand, the average specific powers are comparable for all cases considered.

## NOMENCLATURE

$q_{mi}$	Langmuir constant (mole/kg) as a function of Temperature
$b_i$	Langmuir constant (1/Pa) as a function of Temperature
$k_{1,i}$	Langmuir isotherm parameter (mole/kg)
$k_{2,i}$	Langmuir isotherm parameter (1/K)
$k_{3,i}$	Langmuir isotherm parameter (1/Pa)
$k_{4,i}$	Langmuir isotherm parameter (K)
$k_a$	parameter to predict CSS profile of TSD method
$k_b$	parameter to predict CSS profile of TSD method
$k_c$	parameter to predict CSS profile of TSD method
$k_d$	parameter to predict CSS profile of TSD method
$C_{pg}$	heat capacity of gas (J/kg/K)
$C_{ps}$	heat capacity of adsorbent (J/kg/K)
$C_{v1L}$	valve coefficient at the feed end of the bed during the 1st step
$C_{v3L}$	valve coefficient at the feed end of the bed during the 3rd step in PSA
$C_{v3U}$	valve coefficient at the product end of the bed during the 3rd step in FVPSA
$C_{v4L}$	valve coefficient at the feed end of the bed during the 4th step in FVPSA
$D_e$	effective diffusivity (m <sup>2</sup> /sec)
$D_{particle}$	particle diameter (m)
$D_x$	dispersion coefficient (m <sup>2</sup> /sec)
$h_i$	heat transfer coefficient (J/m <sup>2</sup> /sec/K)
$-\Delta H$	isosteric heat of adsorption (J/mole)
$i$	a component identifier ("i = 1" denotes CO <sub>2</sub> , "i = 2" is N <sub>2</sub> )
$K_L$	effective axial thermal conductivity (J/m/sec/K)

L	bed length (m)
Mw	molecular weight
n	number of elements for finite difference method
P	total pressure (Pa)
$P_{STP}$	pressure at standard condition ( $10^5$ Pa) (Pa)
$P_{feed}$	feed pressure (Pa)
$P_i$	partial pressure (Pa)
$P_{purge}$	purge pressure (Pa) in PSA
$P_{pro}$	Cocurrent blowdown product pressure (Pa) in FVPSA
$P_{reg}$	Countercurrent regeneration pressure (Pa) in FVPSA
$P_{initial}$	Initial pressure within the bed (Pa)
$q_i$	solid phase concentration (mol/kg)
$q_i^*$	amount of adsorption of component i in equilibrium state of mixture
R	universal gas constant (J/mol/K)
q	state variable
$R_{bed}$	bed radius (m)
$R_{particle}$	particle radius (m)
t	time (sec)
$t_{cycle}$	cycle time (sec)
$t_P$	pressurization time (sec)
$t_A$	adsorption time (sec)
$t_{DP}$	depressurization time (sec) in PSA
$t_{PRO}$	cocurrent blowdown product time (sec) in FVPSA
$t_R$	purge time in PSA and regeneration time (sec) in FVPSA
T	gas temperature within the bed (K)
$T_{wall}$	column wall temperature (K)
$T_{STP}$	temperature at standard condition (298.15K) (K)
$T_{feed}$	feed temperature (K)
u	superficial gas velocity (m/sec)
$u_{ads}$	inlet feed gas velocity at the feed end of the bed during the adsorption step (m/sec)
$u_{feed}$	inlet feed gas velocity at the feed end of the bed during the adsorption step (m/sec)
$u_{purge}$	inlet purge gas velocity at the product end of the bed during the purge step (m/sec)

$u_{\text{reg}}$	inlet purge gas velocity at the product end of the bed during the purge step (m/sec)
$w$	constraints
$y_f$	feed mole fraction
$y_i$	mole fraction of component $i$
$z$	the axial position (m) or state variable

### Greek letters

$\varepsilon$	CSS tolerance which is a very small value
$\mu$	gas viscosity (kg/m/sec)
$\rho_{\text{bed}}$	bed density (kg/m <sup>3</sup> )
$\varepsilon_{\text{bed}}$	bed void
$\rho_{\text{gas}}$	gas density (kg/m <sup>3</sup> )
$\Delta H_i$	isosteric heat of adsorption (J/mol) of the component $i$
$\rho_{\text{particle}}$	particle density (kg/m <sup>3</sup> )
$\rho_{\text{wall}}$	wall density (kg/m <sup>3</sup> )
$\varepsilon_t$	total void fraction
$\phi$	representative of mole fraction ( $y$ ), adsorption amount ( $q$ ) and temperature ( $T$ )
$\Phi$	objective function

## References

1. Siriwardane, R. N<sub>2</sub>/CO<sub>2</sub> isotherm data, NETL, DOE, 2004.
2. Ko, D.; Siriwardane, R.; Biegler, L. T. Optimization of PSA using Zeolite 13x for CO<sub>2</sub> Sequestration. 2002 AIChE Annual meeting, Nov. 6, **2002**, Indianapolis, Indiana, USA
3. Ko, D.; Siriwardane, R.; Biegler, L. T. Optimization of a pressure-swing adsorption process using zeolite13x for CO<sub>2</sub> sequestration. *Ind. Eng. Chem. Res.* **2003**, *42*, 339-348
4. Alders, J. G. M. *Energy Conver. Mgmt.* **1992**, *33*(5-8), 283-286
5. Kessel, L.B.M. et al. IGCC power plant: CO<sub>2</sub> removal with moderate temperature adsorbents, final report. TNO report R98/135. 2002
6. PICHTR, CO<sub>2</sub> ocean sequestration: field experiment <http://www.co2experiment.org>, **2001**.
7. Park, J.-H.; Beum, H.-T.; Kim, J.-N.; Cho, S.-H., Numerical analysis on the power consumption of the PSA process for recovering CO<sub>2</sub> from flue gas. *Ind. Eng. Chem. Res.* **2002**, *41*, 4122-4131.
8. IEA Greenhouse R&D program, Carbon dioxide capture from power stations <http://www.ieagreen.org.uk/capt5.htm>, **1994**.
9. Skarstrom, C. W. Method and apparatus for fractionating gaseous mixtures by adsorption. US Patent No. 2944627. **1960**.
10. Marsh, W. D.; Pramuk, F. S.; Hoke, R. C.; Skarstrom, C. W. Pressure equalization depressurizing in heatless adsorption. US Patent No. 3 142 547. **1964**.
11. Berlin, N. H. Method fo r providing an oxygen-enriched environment, US Patent No. 3 280 536. **1966**.
12. Wagner, J. L. Selective adsorption process. US Patent No. 3 430 418. **1984**.
13. Ruthven, D. M. *Principles of adsorption and adsorption processes*. New York: Wiley. **1984**.
14. Yang, R. T. *Gas separation by adsorption processes*. Boston: Butterworths. **1987**.
15. Ruthven, D. M.; Farooq, S.; Knaebel, K. S. *Pressure swing adsorption*. New York: VCH Publishers. **1994**.
16. Chou, C.-T.; Ju, D.-M.; Chang S.-C. Simulation of a fractionated vacuum swing adsorption process for air separation. *Separation science and technology*, **1998**, *33* (13),

2059-2073.

17. Sircar, S.; Zondlo, J. W. US Patent 4,013,429. **1997**.
18. Sircar, S.; Hanley, B. F. Fractionated vacuum swing adsorption process for air separation. *Separation science and technology*, **1993**, 28 (17&18), 2553-2566.
19. Chou, C.-T.; Huang, W.-C. Incorporation of a valve equation into the simulation of a pressure swing adsorption process. *Chemical Engineering Science*, **1994**, 49 (1), 75-84.
20. Process Systems Enterprise Ltd. gPROMS introductory user's guide (release 2.3.1). June 2004.
21. Process Systems Enterprise Ltd. gPROMS advanced user guide (release 2.3). February 2004.
22. Jiang, L.; Biegler, L. T.; Fox, V. G. Simulation and optimization of pressure-swing adsorption systems for air separation. *AIChE Journal*, **2003**, 49(5), 1140-1157.
23. Kim, W.-G.; Yang, J.; Han, S.; Cho, C.; Lee, C.-H.; Lee, H. Experimental and theoretical study on H<sub>2</sub>/CO<sub>2</sub> separation by a five-step one-column PSA process. *Korean J. of Chem. Eng.*, **1995**, 12(5), 503-511.